J. Fluid Mech. (2004), *vol.* 506, *pp.* 315–330.
DOI: 10.1017/S0022112004008493 Printed in the United Kingdom

Vapour extraction from a water-saturated geothermal reservoir

By GEORGE G. TSYPKIN[1] AND ANDREW W. WOODS[2]

[1]Institute for Problems in Mechanics, RAS, Moscow, Russia

[2]BP Institute, University of Cambridge, Madingley Rise, Cambridge, CB3 0EZ, UK

(Received 7 April 2003 and in revised form 21 December 2003)

We examine the decompression and associated flow of water through a high-pressure permeable rock towards a well of low pressure. Using a series of new analytical similarity solutions, and some asymptotic simplifications, we explore the controls on the vaporization as a function of (i) the pressure jump from the far field to the well; (ii) the initial superheat of the reservoir and (iii) the permeability of the system. We find that for a sufficiently large pressure decrease, the liquid becomes superheated and boils, leading to venting of vapour into the well. For a low-permeability system, the flux of liquid from the far field is rate limiting and a sharp boiling interface develops ahead of the well. However, in higher-permeability rock, the flux of water from the far field increases and there is insufficient heat conducted from the far field in order to boil this water. The boiling front is then located at the well, while the fluid ahead of the boiling front may become superheated leading to formation of a two-phase zone which spreads outwards from the well.

1. Introduction

In many geothermal systems, liquid is stored at high pressure in high temperature subsurface permeable rocks. If a fracture or well intersects such a high pressure layer, it will form a localized region of lower pressure. In high-temperature geothermal systems this decrease in fluid pressure may lead to superheating of the liquid and ultimately to the formation of vapour. Also, as the liquid decompresses, a flow will develop towards the region of low pressure (figure 1). This process is important for understanding both natural fumarolic activity, in which steam vents from the ground, and in the industrial context of geothermal power production, in which it is, important to quantify the flux of vapour which may be produced from a reservoir (Brownell, Garg & Pritchett 1977; Faust & Mercer 1979; Garg & Pritchett 1988). A number of studies have considered the production of fluid by decompression of a two-phase geothermal system, in which the liquid is just saturated, and hence both liquid and vapour are both present in the far field (O'Sullivan & Pruess 1980; Sorey, Grant & Bradford 1980; O'Sullivan 1981); however, in the present work, we consider the flows which develop through decompression of a liquid-saturated reservoir, in which the pressure in the far field is sufficiently high that there is only liquid present. The main difference between our work and preceding work is thus that we consider a liquid-filled permeable rock whose initial pressure is in excess of the boiling pressure. We then explore the flow and phase change produced when the pressure at a well is reduced to a value below the boiling pressure; we find that a localized boiling front advances out into the rock from the well. We use these solutions to determine

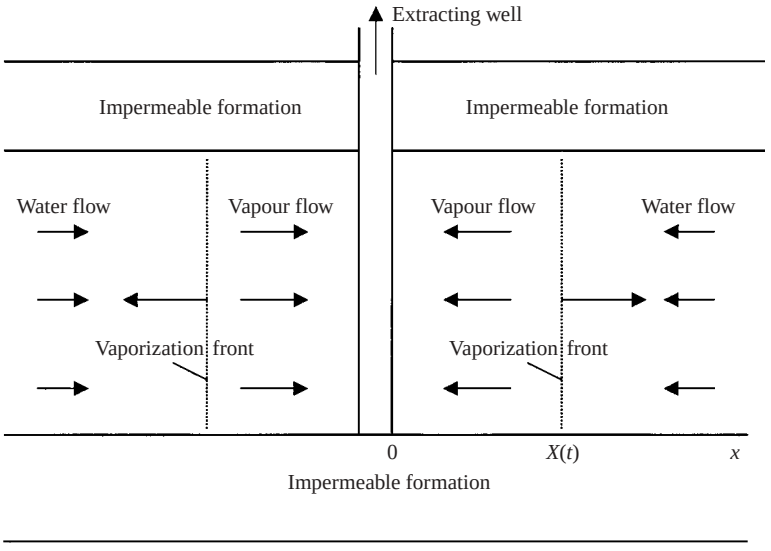

FIGURE 1. The sketch of the problem. The geothermal reservoir is situated between two layers of impermeable rock. Fluid extraction from the well leads to the formation of the vaporization front that separates two single-phase regions.

when the boiling front becomes morphologically unstable (Woods 1999), leading to a finite two-phase region between the pure liquid and pure vapour zones. Since the earlier works of O'Sullivan & Pruess and Sorey *et al.* assume that at the initial time the pressure equals the boiling pressure throughout the rock then the phase change and the formation of a two-phase region occur throughout the rock, and there is no localized boiling front. Although also of interest in geothermal systems, that work is complementary to, but distinct from, the local boiling considered herein.

The balance between the supply of liquid from the far field and the vaporization near the well-bore as the pressure falls depends on the relative distance over which the pressure and temperature fields adjust from the well-bore to the far field. These adjustments occur as diffusion processes. For a low permeability system, the pressure signal will travel slowly, limiting the supply of new liquid. The boiling process is then controlled by the rate at which the cooling front associated with the lower temperature at the well can migrate into the formation, boiling off the water as it advances. This regime has been considered by Tsypkin (1997). In a higher permeability system, the inward liquid supply will be considerably faster. As a result, the flux of heat from the far field to the well may be too small to boil off the advancing liquid. Instead, the liquid migrates right up to the well in liquid form, only vaporizing once it has entered the well.

The purpose of this paper is to examine the decompression and flow of liquid towards a low-pressure well or fracture, accounting for the effects of phase change as appropriate. We present our results by examining a hierarchy of cases. First, in § 2 we examine the decompression and flow of liquid in a high-pressure system, in which the pressure remains in excess of the saturation value as given by the Clausius–Clapeyron relation. Next, in § 3, we show that as the pressure decreases just below the saturation value associated with the reservoir temperature, then the temperature in the liquid advancing towards the well also decreases. In § 4, we show that there is a critical decrease in pressure at the well-bore below which some vaporization of liquid in

the reservoir always occurs, and we then examine the stability of these solutions to superheating of the liquid zone ahead of the pure liquid boiling front. Finally, we draw some conclusions and consider the application of our work.

2. Water extraction at constant temperature

We consider the decompression and flow of pure water from a high-temperature water-saturated geothermal reservoir with constant initial pressure, P_0, and temperature, T_0, and well-pressure, P_w. To prevent boiling, the pressure in the well P_w should be larger than the saturation pressure, $P_f(T_o)$, associated with the far-field temperature of the reservoir $P_w > P_f(T_0)$.

The flow through the permeable rock is governed by Darcy's law (Scheidegger 1974),

$$\boldsymbol{v}_w = -\frac{k}{\mu_w}\,\mathrm{grad}P,$$

coupled with the relation for the conservation of mass

$$\phi\frac{\partial \rho_w}{\partial t} + \mathrm{div}\ \rho_w \boldsymbol{v}_w = 0,$$

and a relation for the dependence of water density on pressure

$$\rho_w = \rho_{w0}[1 + \alpha(P - P_0)].$$

Here, α is the water compressibility coefficient, v is the Darcy or transport velocity, ϕ the porosity, k the permeability, μ the viscosity, P the pressure and ρ the density. In this work, α, ϕ, μ and k are taken to be constants. The subscript w refers to the properties of the water.

The system of equations can be expressed as an equation for the pressure.

$$\frac{\partial P}{\partial t} - \frac{k}{\phi\mu_w}(\mathrm{grad}\ P)^2 = \frac{k}{\phi\alpha\mu_w}\Delta P. \tag{2.1}$$

As long as the pressure is less than the critical pressure for water then

$$\alpha P < 0.75 \times 10^{-9} \times 3 \times 10^7 \ll 1. \tag{2.2}$$

Thus, the nonlinear term on the left-hand side of equation (2.1) is much smaller than the right-hand side and so the equation for pressure evolution can be simplified to the form

$$\frac{\partial P}{\partial t} = \kappa_1 \Delta P \quad \text{where} \quad \kappa_1 = \frac{k}{\phi\alpha\mu_w}. \tag{2.3}$$

2.1. *Similarity solutions*

We consider one-dimensional flow in an unbounded reservoir, $x > 0$. We assume that at the extraction well, $x = 0$, the pressure has value P_w. Thus, the boundary and initial conditions have the form

$$x = 0: \quad P = P_w, \quad t = 0: \quad P = P_0. \tag{2.4}$$

For the one-dimensional extraction problem with constant initial pressure and boundary pressure there is a similarity solution

$$P = P(\xi), \quad \xi = \frac{x}{2\sqrt{\kappa_1 t}}, \tag{2.5}$$

given by

$$P(\xi) = P_0 + (P_w - P_0)\mathrm{erfc}(\xi), \tag{2.6}$$

where $\mathrm{erfc}(z)$ is the complementary error function

$$\mathrm{erfc}(\xi) = 1 - \frac{2}{\sqrt{\pi}} \int_0^{\xi} \mathrm{e}^{-z^2}\, \mathrm{d}z. \tag{2.7}$$

This solution identifies that the flow is driven by the effective diffusion of pressure through the matrix, and that the mass flux decreases at a rate proportional to $t^{-1/2}$.

3. Water extraction with cooling near the well

If the pressure in the well, P_w, is smaller than the saturation pressure associated with the far-field reservoir temperature, $P_w < P_f(T_0)$, then boiling occurs in the well. The phase transition process in the well is complex, but in the simplest case we assume that, in the well, the phase transition realizes the local equilibrium temperature $T = T(P_w)$. Near the well, the temperature of the fluid and rock decreases in order to supply heat to the well through conduction and drive the phase change. If the reservoir pressure falls even further, then eventually some boiling will occur in the rock itself near the well, and we consider this in § 4. The present section is only concerned with the case in which the temperature falls in the neighbourhood of the well.

The temperature distribution in the rock is given from the conservation of energy (Brownell *et al.* 1977; Woods & Fitzgerald 1993)

$$\left.\begin{aligned} &(\rho C)_1 \frac{\partial T}{\partial t} + \rho_w C_w \boldsymbol{v}_w \ \mathrm{grad}\ T = \ \mathrm{div}\ (\lambda_1\ \mathrm{grad}\ T), \\ &\text{where} \\ &\lambda_1 = \phi\lambda_w + (1-\phi)\lambda_s,\ (\rho C)_1 = \phi\rho_w C_w + (1-\phi)\rho_s C_s, \end{aligned}\right\} \tag{3.1}$$

with C representing the specific heat, T the temperature, and λ the thermal conductivity while the subscripts s and w refer to properties of the porous matrix and water, respectively. In this equation, the fluid and rock are assumed to have the same temperature locally, owing to thermal diffusion between the solid and fluid, as is valid in the limit of such slow flows (Woods and Fitzgerald, 1993).

Combining the heat conservation equation with Darcy's law we obtain an equation relating the temperature and pressure

$$(\rho C)_1 \frac{\partial T}{\partial t} - \frac{k}{\mu_w} \rho_w C_w \mathrm{grad} P\ \mathrm{grad}\ T = \lambda_1 \Delta T. \tag{3.2}$$

Equations (3.1) and (3.2) describe heat and mass transfer in the water-saturated permeable porous rock. To solve these equations, we apply initial and boundary conditions for the pressure and temperature

$$x = 0: \quad P = P_w, \quad T = T_w \equiv T_f(P_w), \qquad t = 0: \quad P = P_0, \quad T = T_0. \tag{3.3}$$

3.1. *Similarity solution*

As in § 2, there is no independent length scale for the liquid flow, and so we expect the flow to be self-similar, with

$$P = P(\zeta), \quad T = T(\zeta) \ \text{ where } \qquad \zeta = \frac{x}{2\sqrt{a_1 t}}, \quad a_1 = \frac{\lambda_1}{(\rho C)_1}. \tag{3.4}$$

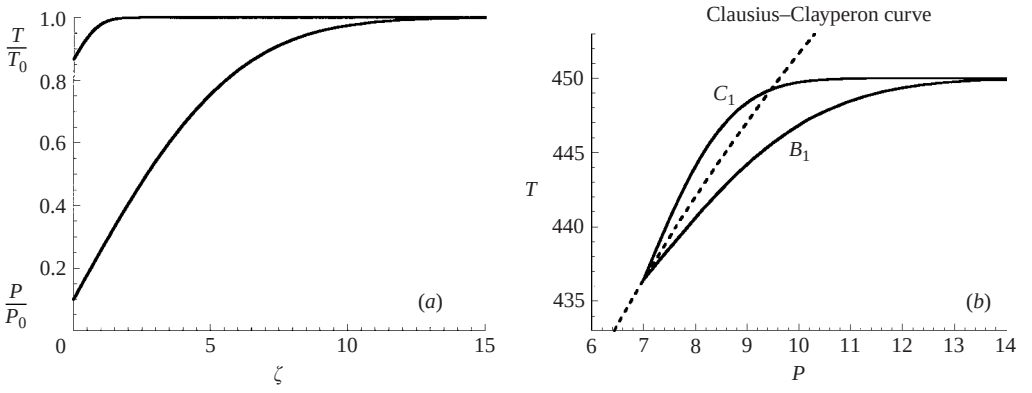

FIGURE 2. (*a*) Typical distribution of the temperature and pressure functions. $T_0 = 450\,\mathrm{K}$, $P_0 = 2 \times 10^6\,\mathrm{Pa}$, $P_w = 2 \times 10^5\,\mathrm{Pa}$, $\phi = 0.2$, $k = 10^{-18}\,\mathrm{m}^2$. (*b*) Typical trajectories in Clausius–Clapeyron plane for water extraction with boiling in the well. $T_0 = 450\,\mathrm{K}$, $P_0 = 8 \times 10^6\,\mathrm{Pa}$, $P_w = 7 \times 10^5\,\mathrm{Pa}$, $\phi = 0.2$; B_1: $k = 3 \times 10^{-17}\,\mathrm{m}^2$, C_1: $k = 5 \times 10^{-17}\,\mathrm{m}^2$.

Here, a_1 denotes the mass averaged thermal diffusivity of the liquid and porous matrix. The pressure distribution has the same solution as in § 2, equation (2.5). The temperature profile in the water region can be simplified by noting that there is a large difference between the typical length scales, L_T and L_P, over which the temperature and pressure fields vary

$$L_T \sim \sqrt{a_1 t}, \quad L_P \sim \sqrt{\kappa_1 t}. \tag{3.5}$$

The thermal diffusivity $a_1 \sim 10^{-6}$ while the pressure diffusivity has the form

$$\kappa_1 = \frac{k}{\phi \alpha \mu_w} \sim \frac{k}{0.2 \times 0.5 \times 10^{-9} \times 10^{-4}} \sim k \times 10^{14}, \tag{3.6}$$

and so for $k \gg 10^{-20}\,\mathrm{m}^2$, $a_1 \ll \kappa_1$ and $L_T \ll L_P$. Hence, the variation in temperature takes place in a layer that has similarity length $\zeta \sim 1$ while the pressure changes over a length $\zeta \sim (a_1/\kappa_1)^{-1/2} \gg 1$. We can therefore approximate the pressure gradient as being constant across the thermal boundary layer near the well

$$\frac{\partial P}{\partial x} = -\frac{P_w - P_0}{\sqrt{\pi \kappa_1 t}} \exp(-\zeta^2 a_1/\kappa_1) \approx -\frac{P_w - P_0}{\sqrt{\pi \kappa_1 t}}. \tag{3.7}$$

Also the nonlinear heat conservation equation may be linearized in the region $\zeta = O(1)$

$$\frac{\partial T}{\partial t} + \frac{\rho_w C_w}{(\rho C)_1} \frac{k}{\mu_w} \frac{P_w - P_0}{\sqrt{\pi \kappa_1 a_1}} \sqrt{\frac{a_1}{t}} \frac{\partial T}{\partial x} = a_1 \frac{\partial^2 T}{\partial x^2}. \tag{3.8}$$

The similarity solution for the temperature then has the form

$$T(\zeta) = T_0 + (T_w - T_0) \frac{\mathrm{erfc}\,(\zeta + A_T)}{\mathrm{erfc}(A_T)}, \qquad A_T = \frac{\rho_w C_w}{(\rho C)_1} \frac{k}{\mu_w} \frac{P_0 - P_w}{\sqrt{\pi \kappa_1 a_1}}. \tag{3.9}$$

Figure 2(*a*) illustrates the distribution of temperature and pressure as a function of distance from the well for typical values of the main parameters shown in table 1 (Grigoriev 1997). The figure demonstrates the large difference in the length scales of the temperature and pressure gradients for rock of permeability $k = 10^{-18}$ m^2. Figure 2(*b*) illustrates the variation of temperature as a function of pressure for two different values of permeability. In each case, the variation of the temperature with

$\rho_w = 0.89 \times 10^3\ \mathrm{kg\,m^{-3}}$	$\rho_s = 2.6 \times 10^3\ \mathrm{kg\,m^{-3}}$
$\mu_w = 1.5 \times 10^{-4}\ \mathrm{Pa\,c}$	$\mu_v = 1.6 \times 10^{-5}\ \mathrm{Pa\,c}$
$C_w = 4390\ \mathrm{J\,kg^{-1}K^{-1}}$	$C_s = 920\ \mathrm{J\,kg^{-1}K^{-1}}$
$\alpha = 7.5 \times 10^{-10}\ \mathrm{Pa^{-1}}$	$P_a = 10^5\ \mathrm{Pa}$
$R = 461\ \mathrm{J\,kg^{-1}\ K^{-1}}$	$q = 2 \times 10^6\ \mathrm{J\,kg^{-1}}$
$\lambda_w = 0.7\ \mathrm{W\,m^{-1}K^{-1}}$	$\lambda_s = 2\ \mathrm{W\,m^{-1}K^{-1}}$

TABLE 1. Typical values of main parameters.

pressure is compared with the variation of the saturation temperature with pressure. It is seen that for the small value of permeability (curve B_1) the liquid remains cooler than the saturation pressure everywhere in the porous rock. However, in the case of larger permeability (curve C_1) the water temperature exceeds the saturation temperature and we expect that the water will become superheated in the rock.

4. Boiling within the permeable rock

If the pressure in the well is sufficiently small, then there will be some boiling of water in the rock and a vapour saturated region will develop adjacent to the extraction well. Although the hot water and vapour move towards the well, the vaporization front migrates away from the well (figure 1). The heat required to drive the vaporization diffuses towards the front from the liquid zone ahead of the front, so that the temperature at the vaporization front is smaller than in the far field. Since there is no heat sink in the extraction well, then to good approximation, the vapour zone is isothermal since the fluid reaches the well in the vapour state. We now develop a simplified mathematical model to describe this process. In the vapour region, the conservation of mass, Darcy's law and the equation of state have the form

$$\phi \frac{\partial \rho_v}{\partial t} + \mathrm{div}\ \rho_v \boldsymbol{v}_v = 0, \qquad \boldsymbol{v}_v = -\frac{k}{\mu_v}\ \mathrm{grad}\ P, \qquad P = \rho_v R T. \tag{4.1}$$

Here, we assume that the vapour behaves as a perfect gas with R the gas constant for the vapour, and the subscript v refers to the properties of the vapour. Combining equations (4.1), we find that the pressure evolves according to the relation

$$\frac{\partial P}{\partial t} - \frac{k}{\phi \mu_v}(\mathrm{grad}\ P)^2 = \frac{k}{\phi \mu_v} P \Delta P. \tag{4.2}$$

We assume that the vaporization occurs across a narrow front which slowly migrates outwards from the well. The boundary conditions across this front may be found using the local conservation of mass and energy, assuming that all phases are in local thermodynamic equilibrium. These relations are supplemented by the Clausius–Clapeyron curve which determines the vaporization temperature as a function of the pressure, $T = T_f(P)$. If we denote the pressure and temperature at the boiling front by P_* and T_*, then the conservation of mass and heat across the vaporization front take the form

$$\phi \left(1 - \frac{P_*}{\rho_w R T_*}\right) V_n = \frac{k P_*}{\mu_v \rho_w R T_*}(\mathrm{grad}\ P)_{n-} - \frac{k}{\mu_w}(\mathrm{grad}\ P)_{n+}, \tag{4.3}$$

$$\phi q \rho_w V_n = \lambda_+ (\mathrm{grad}\ T)_{n+} - \frac{k q \rho_w}{\mu_w}(\mathrm{grad}\ P)_{n+}, \tag{4.4}$$

$$\text{where} \quad T_+ = T_- = T_*, \qquad P_+ = P_- = P_*. \tag{4.5}$$

For the purposes of calculation, we approximate the Clausius–Clapeyron curve with the relation (Tsypkin 1997)

$$\ln\frac{P_*}{P_a} = A + \frac{B}{T_*}, \qquad A = 12.512, \quad B = -4611.73, \quad P_a = 10^5\,\text{Pa}, \tag{4.6}$$

which is very accurate for pressures in the range $3 \times 10^7 > P > 2 \times 10^5$.

As for the liquid region (§ 3), in the vapour region, the effective pressure diffusion coefficient $kP_*/\mu_w\phi$ is much greater than the thermal diffusivity, a_1. The thermal diffusivity in the liquid zone determines the length scale of the vaporization front ahead of the well since the vaporization is controlled by heat conduction towards the well from the liquid. Therefore, as the vaporization front migrates outwards from the well, the pressure in the vapour region is able to adjust rapidly so that at all times there is a nearly constant vapour flux, independent of position. Hence, in the vapour region, the pressure may be approximated by the form

$$\text{div}(P\,\text{grad}\,P) = 0. \tag{4.7}$$

4.1. *Similarity solutions*

As in §§ 2 and 3, there is no external lengthscale in the problem, and so the system admits similarity solutions (3.9) in which the location of the boiling front is given by

$$X(t) = 2\gamma\sqrt{a_1 t}. \tag{4.8}$$

In the vapour region, the pressure distribution is given by

$$P(\zeta) = \sqrt{(P_w)^2 + [P_*^2 - (P_w)^2]\frac{\zeta}{\gamma}} \quad (0 < x < X(t)), \tag{4.9}$$

while the pressure and temperature distributions in the water region $X(t) < x < \infty$ are derived from equations (2.6) and (3.9) and have the form

$$\left.\begin{aligned} P(\zeta) &= P_0 + (P_* - P_0)\frac{\text{erfc}\left(\zeta\sqrt{a_1/\kappa_1}\right)}{\text{erfc}\left(\gamma\sqrt{a_1/\kappa_1}\right)}, \\ T(\zeta) &= T_0 + (T_* - T_0)\frac{\text{erfc}(\zeta + A_T)}{\text{erfc}(\gamma + A_T)}, \\ A_T &= \frac{\rho_w C_w}{(\rho C)_1}\frac{k}{\mu_w}\frac{P_0 - P_*}{\sqrt{\pi\kappa_1 a_1}}, \end{aligned}\right\}, \tag{4.10}$$

where P_* and T_* are the interface pressure and temperature. By combining the above solutions (4.9) and (4.10) with the boundary conditions (4.3)–(4.6) we obtain two transcendental equations for the dimensionless quantities γ, $\hat{T}_* = T_*/T_0$, $\hat{P}_* = P_*/P_0$

$$\sqrt{\pi}\,\frac{a_1\ \phi\ q\ \rho_w}{T_0\ \lambda_1}\gamma\ - \frac{k\ q\ \rho_w\ P_0}{\mu_w\ T_0\ \lambda_1}\sqrt{\frac{a_1}{\kappa_1}}(\hat{P}_* - 1)\frac{\exp(-\gamma^2\ a_1/\kappa_1)}{\text{erfc}(\gamma\sqrt{a_1/\kappa_1})} + (\hat{T}_* - 1)\frac{\exp(-(\gamma + A_T)^2)}{\text{erfc}(\gamma + A_T)} = 0, \tag{4.11}$$

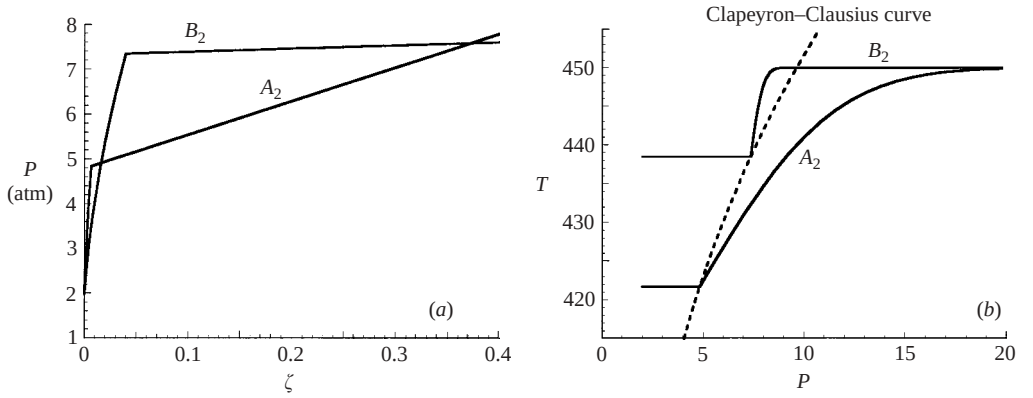

FIGURE 3. (a) Variation of the water pressure as a function of dimensionless position ζ at different values of initial pressure (b). Variation of the temperature (solid line) and phase transition temperature (dashed lines) as a function of pressure in phase plane. $T_0 = 450\,\mathrm{K}$, $P_w = 2 \times 10^5\,\mathrm{Pa}$, $\phi = 0.2$; $k = 10^{-17}\,\mathrm{m}^2$, B_2: $P_0 = 2 \times 10^6\,\mathrm{Pa}$, A_2: $P_0 = 1.4 \times 10^7\,\mathrm{Pa}$.

$$\frac{\sqrt{\pi a_1 \kappa_1}\ \phi \mu_w}{k P_0}\left(1 - \frac{P_0}{\rho_w\ R\ T_0}\ \frac{\hat{P}_*}{\hat{T}_*}\right)\gamma - (\hat{P}_* - 1)\frac{\exp(-\gamma^2 a_1/\kappa_1)}{\mathrm{erfc}(\gamma\sqrt{a_1/\kappa_1})} - \frac{1}{4\ \gamma\ \hat{T}_*}\sqrt{\pi\frac{\kappa_1}{a_1}}\ \frac{\mu_w}{\mu_v}\ \frac{P_0}{\rho_0\ R\ T_0}\ \left[\hat{P}_*^2 - \left(\frac{P_w}{P_0}\right)^2\right] = 0. \quad (4.12)$$

These two equations, together with the condition that the temperature at the interface, T_*, is related to the pressure, P_*, through the Clausius–Clapeyron relation (4.6) was solved numerically for typical values of the parameters. The structure of solutions is dependent on the reservoir pressure and, in figure 3, we illustrate the variation of the pressure with distance from the well and the temperature as a function of pressure on the (T, P) phase plane, for two values of reservoir pressure, 2×10^6 Pa (curve B_2) and 1.4×10^7 Pa (curve A_2), with the same fixed well pressure, 2×10^5 Pa. The discontinuity in the gradient of each curve corresponds to the position of the front.

Figure 3(a) identifies that for large reservoir pressure, there is an associated increase in pressure gradient in the water zone which leads to an increase in the water flux supplied to the vaporization front. This reduces the rate of outward migration of the front and the motion is characterized by a smaller value of the phase transition pressure. Figure 3(b) compares the temperature (solid line) with the saturation temperature (dashed line) as a function of pressure. The saturation temperature is calculated from the Clausius–Clapeyron relation. The figure shows that for the larger reservoir pressure (curve A_2), the saturation temperature exceeds the water temperature everywhere in the liquid zone. However, as in case C_1 of figure 2(b), for the smaller reservoir pressure (curve B_2), the water temperature exceeds the saturation temperature just ahead of the boiling front. The formal mathematical solution may therefore be unstable since there is a region of water in which the temperature is in excess of the Clausius–Clapeyron temperature for that pressure. Such superheating of the water ahead of the vaporization front causes the solution to become unstable and we consider this in the next section.

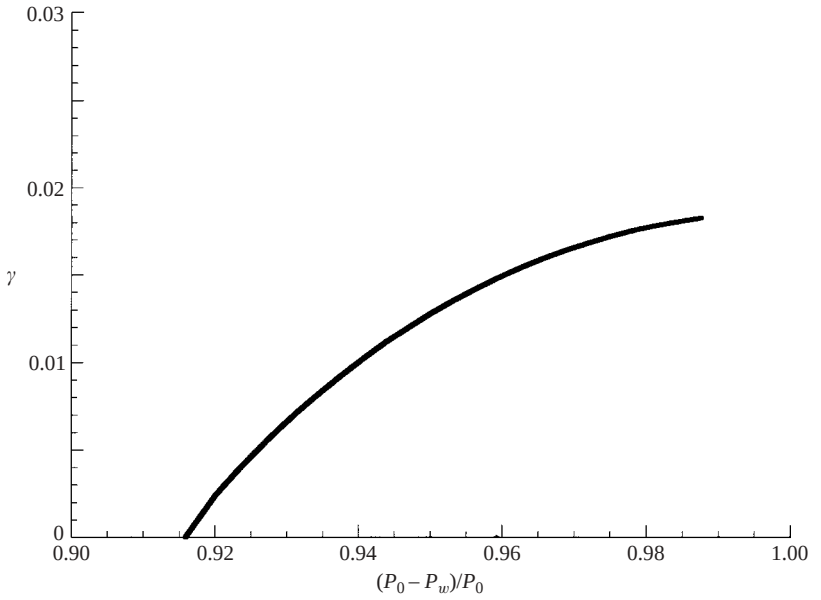

FIGURE 4. Variation of γ as a function of the difference between the fixed reservoir pressure and the well pressure. As the well pressure falls, the flux from the far field increases and γ increases. $T_0 = 450\,\mathrm{K}$, $\phi = 0.2$; $k = 10^{-17}\,\mathrm{m}^2$, $P_0 = 8 \times 10^6\,\mathrm{Pa}$.

Note that in the vapour zone adjacent to the well, in our approximate solution, the temperature is assumed to remain constant, while the pressure decreases from the saturation value to the well pressure.

Figure 4 illustrates how the speed of the boiling front, as quantified by γ, varies with the well pressure for a given reservoir pressure, 8×10^6 Pa. The figure shows that there is a critical well pressure at which boiling commences, $\gamma = 0$, and as the well pressure falls to progressively smaller values, the boiling rate and hence γ, gradually increase.

4.2. *A simple estimate of the boiling temperature*

In the above solution, the boiling front migrates away from the well at a rate which is limited by thermal diffusion, while the liquid advances towards the well at a rate which is limited by the much larger effective diffusivity of pressure in the liquid saturated porous rock. We therefore anticipate that the absolute rate of migration of the boiling front will be relatively small, and so the flux of liquid into the boiling front will be comparable to the flux of vapour produced at the boiling front. Thus, we expect that condition (4.3) has the dominant balance

$$\frac{\rho_v}{\mu_v}(\mathrm{grad}\ P)_{n-} \approx \frac{\rho_w}{\mu_w}(\mathrm{grad}\ P)_{n+}. \tag{4.13}$$

Analogously, the heat conservation relation (4.4) across the interface has the dominant balance

$$\lambda_+(\mathrm{grad}\ T)_{n+} \approx \frac{kq\rho_w}{\mu_w}(\mathrm{grad}\ P)_{n+}. \tag{4.14}$$

Furthermore, the thickness of the vapour layer around the well is relatively small compared to the region over which the liquid pressure varies, therefore $P_* \sim P_w$. Thus

P_0	T_*	T_{est}	$T_* - T_{est}$	$T_* - T_{est}/T_{est}$
2×10^6	438.48	446.3	−7.82	−0.0175
8×10^6	431.39	433.9	−2.51	−0.0058
1.4×10^7	421.72	421.4	0.32	0.0008

TABLE 2. Accuracy of the formula (4.17) $T_* - T_{est}$ denotes the absolute and $(T_* - T_{est})/T_{est}$ the relative error.

to leading order, the energy conservation law at the boiling front has the form

$$\lambda_+ \frac{\delta T}{L_T} \sim \frac{kq\rho_w}{\lambda_+ \mu_w} \frac{\delta P}{L_P}. \tag{4.15}$$

Since the length scale of the thermal boundary layer near the well $L_T \sim \sqrt{a_1 t}$ is much smaller than that over which the pressure varies $L_P \sim \sqrt{\kappa_1 t}$, we obtain the relation

$$\delta T \sim \frac{kq\rho_w}{\lambda_+ \mu_w} \sqrt{\frac{a_1}{\kappa_1}}\, \delta P. \tag{4.16}$$

This formula gives an estimate for the magnitude of the decrease in temperature in the water region between the boiling front and the far field in the limit that the pressure-driven flow controls the production of vapour. The phase transition temperature is then given by the approximate relation

$$T_{est} \approx T_0 + \frac{kq\rho_w}{\lambda_+ \mu_w} \sqrt{\frac{a_1}{\kappa_1}}\, (P_w - P_0). \tag{4.17}$$

The results of numerical solution of the system of transcendental equations, and these approximate values illustrate the accuracy of the approximate formula (4.17) as shown in table 2.

5. Condition for water superheating in the rock

We have seen in §§ 3 and 4.1 that, in some cases, the liquid may become superheated. This is because ahead of the phase change front as the water pressure decreases the phase transition temperature falls below the far-field temperature of the water. Since the temperature increases over a shorter length scale than the pressure, the liquid may thereby become superheated. Indeed, the liquid will become superheated if, at the boiling front, the temperature gradient is steeper than the gradient of the Clausius–Clapeyron curve. This relation of the water superheating may be written in the equivalent form

$$\frac{\mathrm{d}T}{\mathrm{d}P} > \frac{\mathrm{d}T_f(P)}{\mathrm{d}P}, \tag{5.1}$$

where derivatives are evaluated at the interface. Using (3.5), the left-hand side may be written in the approximate form

$$\frac{\mathrm{d}T}{\mathrm{d}P} \sim \frac{\delta T/L_T}{\delta P/L_P} = \frac{\delta T}{\delta P}\frac{L_P}{L_T} = \frac{T_0 - T_*}{P_0 - P_*}\sqrt{\frac{\kappa_1}{a_1}}. \tag{5.2}$$

Expression (5.2) illustrates that a decrease in permeability or an increase in reservoir pressure P_0 may eliminate the water superheating and suppress the water boiling ahead of the front. Note that the vaporization pressure P_* has the same order

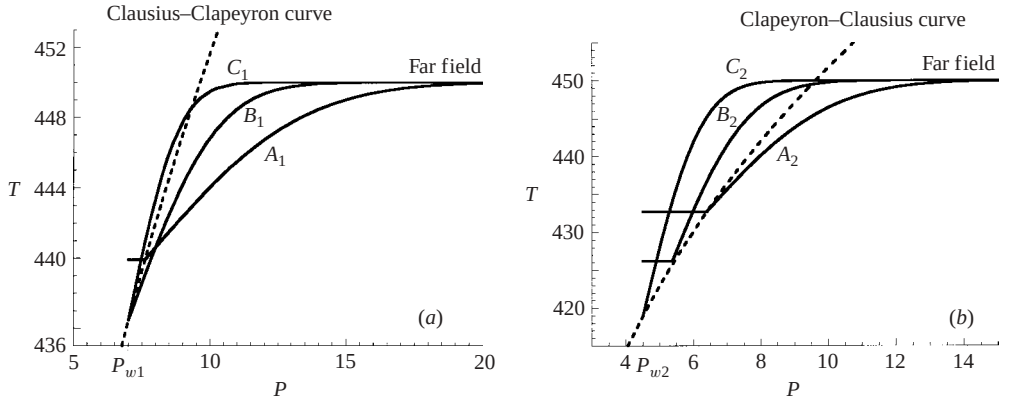

FIGURE 5. Variation of the water temperature (solid lines) and the phase transition temperature (dashed lines) as a function of pressure. $T_0 = 450$ K, $\phi = 0.2$, $P_0 = 8 \times 10^6$ Pa. (*a*) $P_w = 7 \times 10^5$ Pa; $A_1 - k = 4 \times 10^{-18}$ m^2, $B_1 - k = 2.5 \times 10^{-17}$ m^2, $C_1 - k = 5 \times 10^{-17}$ m^2. (*b*) $P_w = 4.5 \times 10^5$ Pa; $A_2 - k = 10^{-17}$ m^2, $B_2 - k = 2.5 \times 10^{-17}$ m^2, $C_2 - k = 5 \times 10^{-17}$ m^2.

as the well pressure P_w and the dominant contribution to denominator $P_0 - P_*$ comes from the reservoir pressure as $P_0 \gg P_* \sim P_w$. Although the well pressure, P_w, is small compared with the reservoir pressure, the vaporization pressure and hence temperature depends strongly on the well pressure. Indeed, an increase in the well pressure P_w prevents the water superheating since it leads to a decrease in $T_0 - T_*$ and therefore the derivative $\mathrm{d}T/\mathrm{d}P$ becomes smaller.

We can check the estimate relation (5.2) by using the exact similarity solution (4.10). Substituting the similarity solutions for temperature and pressure into relation (5.1) we find the condition for superheating at the liquid front has the form

$$-(T_* - T_0)\frac{\exp(-(\gamma + A_T)^2)}{\operatorname{erfc}(\gamma + A_T)} > -\frac{\mathrm{d}T_f(P)}{\mathrm{d}P}\sqrt{\frac{a_1}{\kappa_1}}(P_* - P_0)\frac{\exp(-\gamma^2 a_1/\kappa_1)}{\operatorname{erfc}(\gamma\sqrt{a_1/\kappa_1})}, \quad (5.3)$$

in the case that the there is a finite boiling zone around the well, whereas in the case that there is no boiling zone around the well, the condition for superheating becomes

$$-(T_* - T_0)\frac{\exp\left(-A_T{}^2\right)}{\operatorname{erfc}(A_T)} > -\frac{\mathrm{d}T_f(P)}{\mathrm{d}P}\sqrt{\frac{a_1}{\kappa_1}}(P_* - P_0). \quad (5.4)$$

It is useful to derive a simple estimate for this condition in the case that the boiling front migrates very slowly, $\gamma \ll 1$. In this case, we estimate that

$$A_T = \frac{\rho_w C_w}{(\rho C)_1}\frac{k}{\mu_w}\frac{P_0 - P_*}{\sqrt{\pi\kappa_1 a_1}} \sim \frac{10^{-17}10^7}{10^{-4}\sqrt{10^{-3}10^{-6}}} \sim 3 \cdot 10^{-2} \ll 1, \quad (5.5)$$

and so the condition for superheating (5.4) has the form

$$\frac{T_0 - T_*}{P_0 - P_*}\sqrt{\frac{\kappa_1}{a_1}} > \frac{\mathrm{d}T_f(P)}{\mathrm{d}P}. \quad (5.6)$$

This expression coincides with the estimate (5.2).

6. Suppression of a boiling front in high-permeability rock

As anticipated by the analysis in § 5, figure 5 shows that as the well pressure decreases or the reservoir permeability increases, there is a transition in regime. For

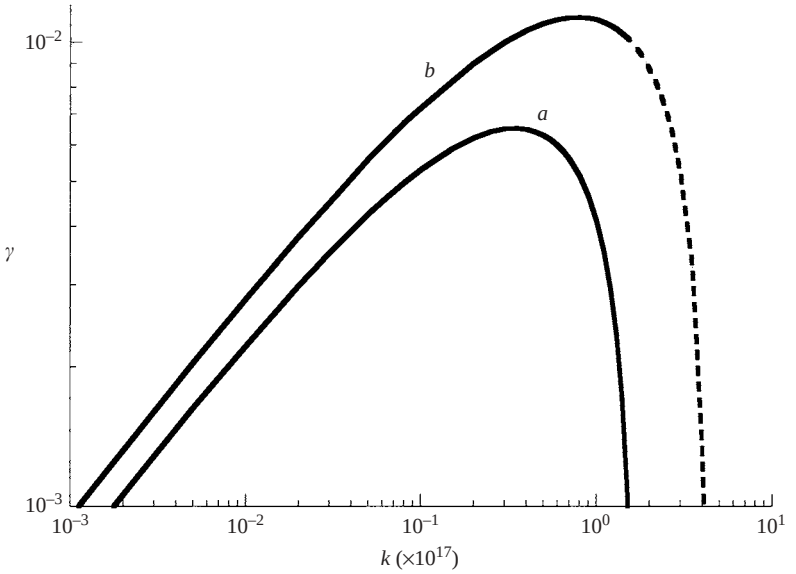

FIGURE 6. Variation of the boiling rate γ as a function of the permeability of the reservoir. Curves are shown for two values of the well pressure, a: $P_w = 5 \times 10^5$ Pa; b: $P_w = 2 \times 10^5$ Pa. The onset of superheating in the liquid is shown by the dashed part of the curve.

large well pressures, there is a simple liquid flow, with a decrease of temperature near the well (curve B_1). For smaller well pressures, a boiling zone develops around the well, as illustrated in the transition from regime B_1 (figure 5a) to regime B_2 (figure 5b). In the case B_2, the liquid zone ahead of the boiling front becomes superheated and unstable. We now explore how the critical points, which delineate the different modes of vaporization, vary with reservoir properties and in particular, the permeability.

Reservoirs with greater permeability have greater effective pressure diffusion coefficient and hence higher liquid flow rates. This tends to decrease the pressure gradient, and lower the interfacial pressure, leading to a tendency for superheating of the liquid ahead of the boiling front (figure 5). Indeed, for sufficiently high permeability, we expect the boiling front to migrate back towards the well bore, while a large zone of superheated liquid will develop in the formation just ahead of the well. We can illustrate the onset of water superheating by considering relation (5.6). Figure 6 illustrates the variation of the boiling rate γ (equation (4.8)) with permeability for two different values of the well pressure for a fixed reservoir pressure. In both cases, it may be seen that the boiling rate initially increases with permeability. This is because the increasing permeability enables a greater flux of liquid to migrate to the well and thereby vaporize. Indeed, from equation (4.11), we expect that for small values of k, the rate of vaporization, as parameterized by γ, should increase as $k^{1/2}$, and this is in very good accord with the results shown in figure 6 for small k. However, as the permeability continues to increase, the increasing flux of liquid from the far field eventually causes the interfacial pressure to decrease towards the well pressure, suppressing the boiling, so that the vaporization front migrates back towards the well bore.

In the figure, we also indicate the critical value of k at which the liquid ahead of the vaporization front becomes superheated. For permeabilities in excess of this value, the value of γ is shown as a dashed line. For the case of a large well pressure

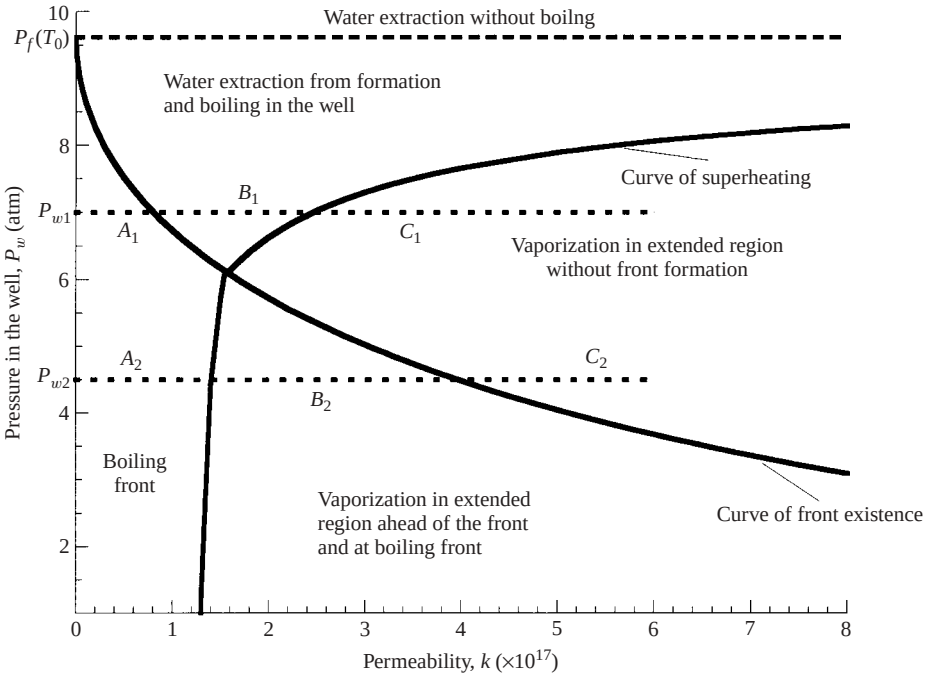

FIGURE 7. Critical diagram illustrating the dependence of the onset of boiling in the reservoir, and the onset of superheating in the reservoir as a function of the reservoir permeability and the well pressure. $T_0 = 450\,\mathrm{K}$, $\phi = 0.2$; $P_0 = 8 \times 10^6\,\mathrm{Pa}$.

(curve *a*), the liquid ahead of the vaporization pressure remains undersaturated for all solutions in which there is a finite boiling zone around the well (e.g. figure 5*a*, curve A_1). This is because the well pressure is similar to the reservoir pressure and thus suppresses the development of any superheating. In this case, superheating only develops at larger permeability, when the model predicts pure liquid flow into the well (e.g. figure 5*a*, curve C_1). In the case of the smaller well pressure (curve *b*, figure 6), the interfacial temperature T_* is smaller and $\mathrm{d}T/\mathrm{d}P$ is larger (see 5.2), and we predict that some superheating develops in the liquid ahead of the boiling front once the permeability exceeds a critical value (figure 5*b*, curve B_2). For larger permeability, no boiling zone develops around the well, but the liquid ahead of the well is again predicted to be superheated (curve C_2, figure 5*b*).

Figure 7 summarizes these results as a regime diagram, illustrating the impact of reservoir permeability on the critical well pressure required for (i) development of a boiling front ahead of the well bore, and also (ii) for which superheating develops in the liquid region. The well pressures and permeabilities of each of the solutions shown in figures 5 and 6 are indicated in figure 7. Figure 7 identifies that five different regions may develop depending on the well pressure and permeability, as indicated on the diagram. The similarity solutions presented earlier in the work apply strictly only to the cases in which the liquid region remains undersaturated or is just saturated.

Relations (5.1) and (4.17) delineate the boundaries between the different vaporization regimes. The condition

$$\frac{\mathrm{d}T}{\mathrm{d}P} = \frac{\mathrm{d}T_f(P)}{\mathrm{d}P} \tag{6.1}$$

separates the regimes in which there is a simple boiling front and in which there is an extended two-phase zone.

In the limit $\gamma \to 0$, relation (4.17) provides the condition for which a boiling front can develop in the rock rather than the case in which boiling only occurs in the well

$$T_f(P_w) = T_0 + \frac{kq\rho_w}{\lambda_+ \mu_w} \sqrt{\frac{a_1}{\kappa_1}} \, (P_w - P_0). \tag{6.2}$$

The point at which both conditions apply can be found by using the Clausius–Clapeyron relation, with $\gamma = 0$ yeilding the relation

$$\frac{T_f(P_w)}{B} \left[1 - \frac{P_0}{P_w}\right] \sqrt{\frac{a_1}{\kappa_1}} - \left[\frac{T_0}{T_f(P_w)} - 1\right] = 0. \tag{6.3}$$

7. Influence of reservoir pressure on boiling regime

In the previous section, we explored the influence of the reservoir permeability on the regime diagram (figure 7), illustrating that for a given reservoir pressure, the boiling regime depends on both the well pressure and the permeability. We found that with small permeability, either a pure boiling front or no boiling occurs in the formation. In contrast, at higher permeability the liquid tends to become superheated ahead of either the well or the boiling front as $\mathrm{d}T/\mathrm{d}P$ increases. This may be understood in terms of the relative length scales over which pressure and temperature change in the liquid region just ahead of the interface. As the permeability becomes smaller, the length scale over which the pressure changes in the liquid ahead of the front becomes smaller, and so the liquid region is able to remain at pressures in excess of the saturation value, even though the temperature is decreasing in this region (e.g. line A_1, figure 5*a*).

A similar physical explanation may be used to interpret the variation of the flow regime with reservoir pressure. Figure 8 illustrates how the critical well pressure for the onset of a boiling front and also for the development of superheated zone in the liquid depend on the reservoir pressure. We find that for a given reservoir pressure, then as the well pressure decreases, the temperature gradient in the liquid zone increases and so $\mathrm{d}T/\mathrm{d}P$ increases until eventually the model predicts formation of a two-phase zone. As the well pressure is decreased further, then we predict that a pure boiling front develops around the well bore, but with the liquid ahead of this front being superheated, and hence out of thermal equilibrium. However, at a particular reservoir pressure, the onset of superheating in the liquid occurs at the same well pressure as that at which a pure boiling front develops around the well. For larger reservoir pressures, we find that as the well pressure is decreased, the formation of the boiling front occurs while the liquid ahead of the front has a temperature less than boiling point.

8. Conclusions

We have examined the pressure-driven flow of liquid from a high-pressure porous rock towards a low-pressure well. Our model accounts for the temperature and phase changes which may occur if the well pressure is smaller than the saturation pressure associated with the reservoir temperature. We have shown that as the well pressure falls below this critical value, initially the temperature and pressure at the well decrease, but there is no phase change in the formation.

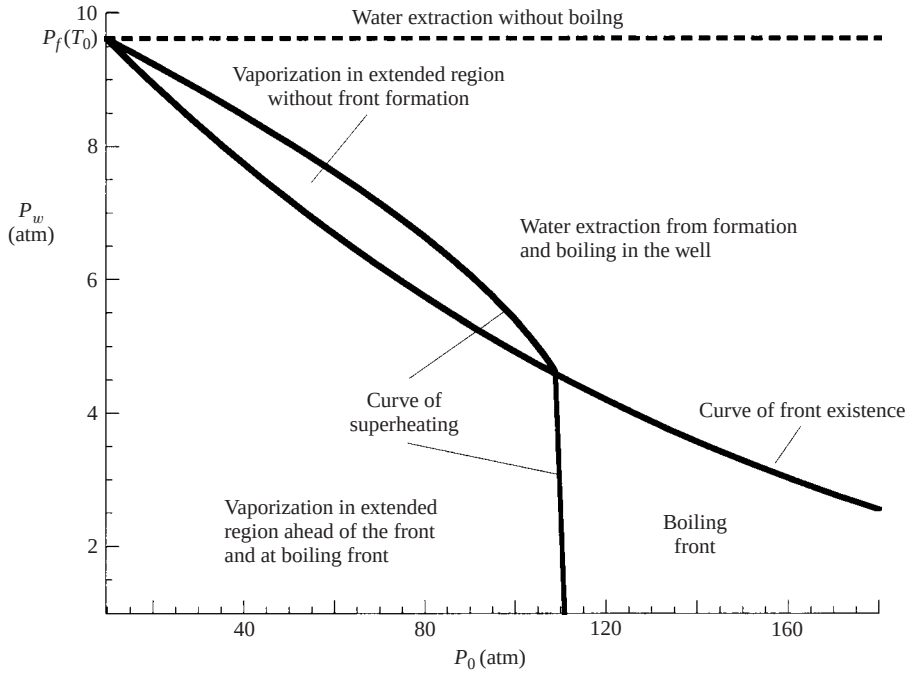

FIGURE 8. Critical diagram illustrating the dependence of the onset of boiling in the reservoir, and the onset of superheating in the reservoir as a function of the initial reservoir pressure and the well pressure. $T_0 = 450$ K, $\phi = 0.2$; $k = 2 \times 10^{-17}$ m^2.

In low-permeability rock, we find that as the pressure decreases further, some boiling commences in the porous rock. For low-permeability rock, the supply of liquid from the far field is suppressed and the boiling occurs in a well-defined zone around the well, with a sharp interface connecting this zone to the liquid further from the well.

However, for larger-permeability rock, we find that as the well pressure decreases below the saturation pressure associated with the reservoir temperature, then the temperature and pressure of the rock adjacent to the well bore lie on the saturation curve. Owing to the much smaller length scale of the thermal boundary layer compared to the pressure boundary layer across which the temperature and pressure of the liquid adjust from the far field to the well, the pressure in the liquid near the well falls below the saturation value and so the liquid becomes superheated. This zone of superheated liquid near the well is unstable and leads to formation of a two-phase boiling zone. A similar superheating process develops in lower-permeability rock, except in that case the superheating only develops at lower well pressures, for which there is already a boiling front, with the superheated zone forming ahead of the boiling front.

The results are of interest for understanding the controls on flow rates both in natural situations, such as the flow from fumaroles in high-temperature geothermal regions, and also in engineered systems in which a high-pressure zone may decompress into a well bore, with the present one-dimensional analysis applying for flow from a confined layer into a near horizontal well. The liquid flux supplied to the well bore has magnitude which varies with time, t, according to the relation $Q = Q_0 t^{-1/2}$ per unit length, where $Q_0 = w(k\Delta P/\mu\phi)^{1/2}$ and w is the width of the fracture. Using the typical values for the permeability, k, and reservoir pressure and temperature, we estimate

that the typical fluxes from a 100 m stretch of a steaming fracture, which vents fluid from a 10 m deep low-permeability zone has magnitude of order $Q_0 \sim 10^{-2} - 10^{-3}\ t^{-1/2}\ \mathrm{m^2\,s^{-1/2}}$.

We are grateful for funding from the BPI which supported G. T. as a senior visiting fellow at the BP Institute.

REFERENCES

Brownell, D. H., Garg, S. K. & Pritchett, J. W. 1977 Governing equations for geothermal reservoirs. *Water Resour. Res.* **13**, 929–934.

Faust, C. R., & Mercer, J. W. 1979 Geothermal reservoir simulation. 1. Mathematical models for liquid- and vapor-dominated hydrothermal systems. *Water Resour. Res.* **15**, 23–30.

Garg, S. K. & Pritchett, J. W. 1988 Pressure interference data analysis for two-phase (water/steam) geothermal reservoirs. *Water Resour. Res.* **24**, 843–852.

Grigoriev, I. S. 1997 *Handbook of Physical Quantities.* Boca Raton.

O'Sullivan, M. J. 1981 A similarity method for geothermal well test analysis. *Water Resour. Res.* **17**, 390–398.

O'Sullivan, M. J. & Pruess, K. 1980 Analysis of injection testing of geothermal reservoirs *Trans. Geoth. Resour. Council* **4**, 401–404.

Scheidegger, A. E. 1974 *The Physics of Flow Through Porous Media.* Toronto.

Sorey, M. L., Grant, M. L. & Bradford, E. 1980 Nonlinear effects in two-phase flow to wells in geothermal reservoir. *Water Resour. Res.* **16**, 767–777.

Tsypkin, G. G. 1997 On water-steam phase transition front in geothermal reservoirs *USA. Proc. Stanford Geotherm. Workshop* **22**, 359–367.

Woods, A. W. & Fitzgerald, S. D. 1993 The generation of vapour through injection of water into a hot rock. *J. Fluid Mech.* **251**, 563–579.

Woods, A. W. 1999 Liquid and vapour flow in superheated rock. *Annu. Rev. Fluid Mech.* **31**, 171–199.